SAND2018-10035J

Pure-Rotational H_2 Thermometry by Ultrabroadband Coherent Anti-Stokes Raman Spectroscopy

Trevor L. Courtney, Alexis Bohlin, Brian D. Patterson and Christopher J. Kliewer[a)]

Combustion Research Facility, Sandia National Laboratories, Livermore, California 94551, USA

Coherent anti-Stokes Raman spectroscopy (CARS) is a sensitive technique for probing highly luminous flames in combustion applications to determine temperatures and species concentrations. CARS thermometry has been demonstrated for the vibrational Q-branch and pure-rotational S-branch of several small molecules. Practical advantages of pure-rotational CARS, such as multi-species detection, reduction of coherent line mixing and collisional narrowing even at high pressures, and the potential for more precise thermometry, have motivated experimental and theoretical advances in S-branch CARS of nitrogen (N_2), for example, which is a dominant species in air-fed combustion processes. Although hydrogen (H_2) is of interest given its prevalence as a reactant and product in many gas-phase reactions, laser bandwidth limitations have precluded the extension of CARS thermometry to the H_2 S-branch. We demonstrate H_2 thermometry using hybrid femtosecond/picosecond pure-rotational CARS, in which a broadband pump/Stokes pulse enables simultaneous excitation of the set of H_2 S-branch transitions populated at flame temperatures over the spectral region 0–2200 cm^{-1}. We present a pure-rotational H_2 CARS spectral model for data fitting and compare extracted temperatures to those from simultaneously collected N_2 spectra in two systems of study: a heated flow and a diffusion flame on a Wolfhard-Parker slot burner. From 300–650 K in the heated flow, the H_2 and N_2 CARS extracted temperatures are, on average, within 2% of the set temperature. For flame measurements, the fitted H_2 and N_2 temperatures are, on average, within 5% of each other from 300–1600K. Our results confirm the viability of pure-rotational H_2 CARS thermometry for probing combustion reactions.

I. INTRODUCTION

a) Author to whom correspondence should be addressed. Electronic mail: cjkliew@sandia.gov.

Coherent anti-Stokes Raman spectroscopy (CARS) remains an important tool for characterizing combustion environments after four decades of CARS thermometry research and application.[1] The coherent nature of the CARS technique affords a dramatic increase of CARS signals over the corresponding spontaneous Raman signals both in absolute strength and in intensity relative to collected background interference. One such interference results from probing the Raman signal in the presence of particulates, which are prevalent in highly luminous soot-forming flames associated with rich combustion conditions. In these environments, the coherent signal of CARS is particularly useful.[2] Although hydrogen (H_2) is generally produced under the rich conditions of applied combustion, nitrogen (N_2) CARS thermometry has been far more extensively developed. N_2 is a dominant species in air-fed combustion reactions, and its linewidth, line-broadening, and other spectroscopic parameters are better known than those of H_2. Thus, the non-combustible N_2 species has been widely used as an indirect probe to report on the spatially and temporally resolved temperature of the combustion reaction. The expansion of the lesser used H_2 CARS methods is desirable, as they provide direct and versatile probing of H_2, which is a common reactant and product of combustion reactions in nitrogen-rich and nitrogen-free combustion environments.

Practical advantages exist for choosing H_2 in CARS thermometry experiments. H_2 is well-suited for vibrational CARS (VCARS) thermometry given the following characteristics: simplicity of H_2 Q-branch spectra with relatively widely spaced and sparse transitions even at flame temperatures, the spectral separation of $\nu = 0 \rightarrow \nu' = 1$ from $\nu = 1 \rightarrow \nu' = 2$ transitions, strength of signal from a large Raman cross section distributed over only a few rotational transitions, and minimal coherent line mixing and collisional narrowing effects at low and moderate pressures.[1] Although the characterization of H_2 linewidths is limited in the literature, initial and more recent

studies have provided essential molecular parameters for developing the spectral model for H_2 temperature fitting.[3-6] Time-resolved CARS measurements have been used to determine H_2 linewidths and broadening coefficients to further models for temperature assignment of H_2 CARS spectra.[7-9] Alternately, H_2 VCARS thermometry has been performed by frequency-domain fitting of the temperature-dependent relative spectral intensities of the well-separated rotational transitions within the first vibrationally excited band.[10-12] Specifically, H_2 VCARS experiments to determine flame temperatures, and in some cases H_2 concentration, have been performed in an ethylene-air Bunsen flame at atmospheric pressure,[13] in the exhaust of a CH_4/air flame under pressure conditions,[14] and in a graphite tube furnace.[15] Shirley, et al. compared H_2 and O_2 VCARS thermometry accuracies across a diffusion flame from a Wolfhard-Parker burner.[1, 16] Later, Hancock et al. used a hydrogen/air flame from a Hencken burner to compare the relative thermometric accuracies of H_2 and N_2 VCARS.[17] Similarly, determining the thermometric accuracy of H_2 pure-rotational CARS (RCARS), with respect to more established N_2 CARS measurements is a goal of this work; however, the key difference is our development and use of an ultrabroadband CARS approach to enable H_2 RCARS thermometry.

Performing RCARS thermometry has garnered interest because of potential advantages over VCARS thermometry. One benefit is that the Raman rotational transitions are, in general, much more widely spaced compared to ro-vibrational transitions, which simplifies data analysis and increases the pressure of the onset of line mixing and collisional narrowing.[1] Another advantage of RCARS is that the rotational Raman spectra of many molecules fall within the same narrow frequency range, and multi-species detection has been demonstrated by several research groups.[18-20] The rotational Raman spectrum of H_2 is an exception to this rule, as the transitions extend much further in frequency. This large spectral range of H_2 rotational lines populated at flame

temperatures has previously prevented the detection of all lines necessary for temperature determination in one signal field. In the only previously published H_2 RCARS thermometry experiments, to our knowledge, Clauss and coworkers employed dual Stokes CARS to compare the simultaneously but separately collected signals from two S-branch transitions.[21 22] Our group has demonstrated a two-beam femtosecond/picosecond (fs/ps) hybrid CARS technique[23-24] capable of collecting the ultrabroadband H_2 S-branch spectrum. Equipped with this broadband technique, we investigate whether the extreme shift of the H_2 S-branch population with temperature could make H_2 more sensitive than other small molecules for RCARS thermometry across a wide range of temperatures.

RCARS thermometry is generally regarded as more accurate than its vibrational counterpart at lower temperatures because of the absence of a significantly populated hot vibrational band. However, once temperatures are high enough, a significant fractional population exists in the first vibrational excited state, and VCARS is regarded as the more accurate technique. For the N_2 molecule, this temperature threshold is around ~1200 K, at which point a Boltzmann analysis shows ~6% of the vibrational population resides in the $v = 1$ initial state. The H_2 molecule has a larger vibrational transition energy, and a temperature of ~2140 K is required to achieve the same 6% population of $v = 1$. Thus, the accuracy advantage of RCARS over VCARS for H_2 thermometry may conceivably exist at even higher temperatures than for N_2 thermometry.

Several advantages of H_2 RCARS thermometry motivate the development and validation of a H_2 RCARS model. With the multiplexed nature of the signal generated in ultrabroadband CARS, robust global fits to the available data across multiple species and molecular manifolds will improve both accuracy and precision of temperature and species concentration measurements. Isolation of the pure-rotational H_2 CARS signal creates an opportunity for detailed studies of

nonequilibrium, or nonthermalized, molecular energy distributions, for which the equipartition theorem is not valid. The wide frequency spacing of the pure rotational states provides a unique test case for exponential gap collisional energy transfer models. Therefore, a time-domain RCARS model for H_2 that can be incorporated into global fits of two-beam ultrabroadband CARS data must be developed and validated to exploit these potential advantages and new directions.

In this paper, we detail the development of RCARS H_2 thermometry, including the experimental setup and methodology, and the theoretical models that we have adapted for fitting of temperature-dependent H_2 S-branch CARS spectra. The resulting temperature profiles from the S-branch spectra of H_2 are compared to the profiles evaluated from simultaneously collected N_2 RCARS spectra to provide an assessment of the accuracy and precision of the H_2 RCARS thermometry. For this assessment, we use both a heated flowing mixture of H_2 and N_2, and a N_2-seeded H_2-fueled diffusion flame from a Wolfhard-Parker slot burner.

II. EXPERIMENT

A. Optical setup

Femtosecond and picosecond amplified laser systems generate the pulses used in these hybrid CARS experiments. The experimental layout is similar to that presented previously,[25] and it is depicted in Fig. 1(a). The mode-locked oscillators seeding the two laser systems are phase locked to the same external 100 MHz radio frequency source, which enables precise electronic timing between the femtosecond and picosecond pulses with low jitter (<1 ps). The pump/Stokes beam originates from the output of a commercial (KM Laboratories Wyvern 1000) Ti:Sapphire regenerative amplifier operating at 1 kHz (780 nm, 45 fs). A 2 mJ portion of amplified 780 nm light is focused into a 310-μm diameter hollow-core fiber that is 1 m in length (Kaleidoscope,

Femtolasers) and housed in a pressure vessel at ~350 Torr Ar. The incoming pulses are frequency broadened via self-phase modulation, and the ~0.8 mJ pulses exiting the fiber are compressed to ~7 fs duration (0.6 mJ/pulse) after a series of reflections from mirrors that impart negative chirp to the pulse. A cylindrical concave silver mirror with 400 mm focal length focuses the horizontally polarized pump/Stokes beam to a vertical sheet. The picosecond probe pulses originate from a high-energy seeded picosecond Nd:YAG regenerative amplifier operating at 20 Hz (~24 mJ/pulse, 65 ps). A half-wave plate rotates the probe polarization to match that of the pump/Stokes beam, and a cylindrical plano-convex lens with 300 mm focal length focuses the beam to a vertical sheet. The two beams intersect at their common horizontal focus; a shallow crossing angle (5°) relaxes the phase-matching conditions for detecting a large range of Raman shifts simultaneously. This 5° intersection of beams with focused diameters of 50 μm full width and half maximum (FWHM) yields an interaction length of ~1 mm. In this work, the sample (labeled S in Fig. 1(a)) is either a N_2-seeded H_2 diffusion flame or a heated flow mixture of N_2 and H_2, as discussed in Section II.B. The temporal delay, τ, of the probe is electronically set to 160 ps to suppress the nonresonant signal fully while still probing relatively early to help balance the detection of N_2 and H_2 with large differences in dephasing times. We determine τ and the probe temporal duration of 65 ps via intensity cross-correlation of the nonresonant spectral portion (integration of <2900 cm^{-1} Raman shifts) of a methane signal.

The imaging and detection scheme (Fig. 1(a)) first involves the isolation of the CARS signal (>40 cm^{-1} Raman shifts) from the probe after transmission through an angle-tuned short-wave-pass filter (Semrock, SP01-561RU-25). The CARS signal generated at the sample vertical sheet interaction region is relay imaged ~1:1 onto the entrance slit of a 0.550 m Czerny-Turner spectrometer (Horiba iHR550, 600 or 2400 grooves/mm grating), and spectrally dispersed onto a

400×1600 pixel (16 μm pixel size), water-cooled (-90° C), back-illuminated CCD array (Andor DU971N-BV). We apply a 2×2 binning in the CCD software, resulting in an array of 200×800 effective pixels with size 32 μm. The collection of each single-shot CCD frame (30 ms exposure time) is triggered by a probe pulse; however, the collection rate of the full frame is electronically limited beyond the 20 Hz laser repetition rate to 6 Hz. A shutter (UniBlitz) at the entrance of the spectrometer is synchronized to the CCD collection to block all additional laser shots.

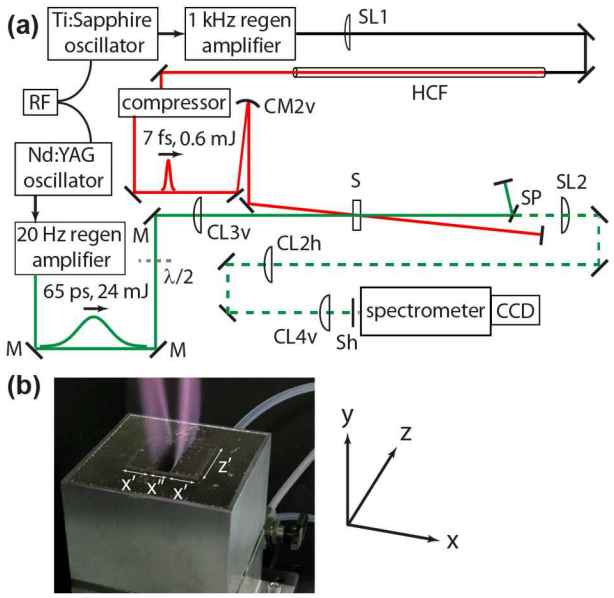

FIG. 1. Two-beam fs/ps CARS experiment. (a) The output of a 1 kHz Ti:Sapphire regenerative amplifier is frequency broadened in a hollow-core fiber (HCF) and compressed with chirped mirrors; each visible/near-IR pulse provides pump and Stokes field interactions. Probe pulses (532 nm) originate from a Nd:YAG regenerative amplifier and transmit through a half-wave plate (λ/2). Polarization-matched beams are focused to intersecting vertical sheets at the sample (S). The CARS signal transmits through a short-pass filter (SP) and is 1:1 relay imaged to the spectrometer and CCD detector. Labels for spherical lenses (SL) and cylindrical lenses (CL) and mirrors (CM) include focal lengths (1, f = 1 m; 2, f = 400 mm; 3, f = 300 mm, 4, f = 75 mm); CL and CM labels also indicate the focusing axis of symmetry (v, vertical; h, horizontal). Sh, shutter; M, dielectric mirror; silver mirrors are unlabeled. (b) Laser beams propagate along z above the Wolfhard-Parker burner with labeled slot dimensions of x′ = 16 mm, x″ = 9 mm, and z′ = 41 mm.

B. CARS measurements

In this work, we demonstrate H_2 RCARS thermometry in a heated flow and across a diffusion flame. The first sample is a mixture of H_2 and N_2 flowing at 1 L/min and 4 L/min, respectively,

that is gradually heated up to ~800 K, as measured by a thermocouple across the flow exit. The second sample is a laminar, nearly two-dimensional flame produced at a fuel-air interface of a Wolfhard-Parker slot burner.[26] Figure 1(b) depicts the burner and its experimental orientation in x (lateral), y (vertical), and z (beam propagation) dimensions. The proportions of three adjacent slots are taken from Ref. [27] and are as follows: 9 × 41 mm (x″ × z′, Fig. 1(b)) center fuel (here, H_2 seeded with N_2) slot and one 16 × 41 mm (x′ × z′, Fig. 1(b)) slot of flowing air on each side of the center slot. Ideally, the gases from each side of a common boundary (here, each z′ = 41 mm edge) rise vertically, diffusing into each other in a laminar flow.[26] The following procedures ensure a steady flame front and a laminar flow: flowing N_2 through an outer shroud that increases each of the x and z burner dimensions to 76.2 mm (also y = 76.2 mm), filling this outer shroud and the air slots with fine sintered bronze honeycomb mesh that is flush with the burner surface, and placing a steel mesh chimney (not shown in Fig. 1(b)) above the burner. The flow rates are 21 L/min for H_2 and 4 L/min for N_2 in the fuel slot and 50 L/min air for the two air slots.

For either sample, the 1D CARS imaging system produces RCARS spectra for both N_2 and H_2, where each CCD row reports on a unique spatial (and thus temperature profile) position in y above the flow tube exit or burner surface. The beam intersection is roughly centered on the stationary flow tube in the x and z dimensions. The exact intersection position for the heated flow is chosen to minimize spatial averaging effects (SAE)[27-28] along the z-dimension of the probe volume, which corresponds to recovered temperatures in close agreement to those reported by the thermocouple. Orienting the Wolfhard-Parker burner such that the probe volume is parallel, or along the 2D flame front has been shown to result in a temperature measurement with little influence from SAE.[27] Because of the steepness of the flame front, our probe region does not span the vertical range necessary to sample the complete reactants-to-products cross section of the

flame, so we translate the burner in the x dimension and measure the temperature at a constant height. The vertical spatial intensity maxima of the pump/Stokes and probe beams are both located ~3.5 mm above the flow tube exit or burner surface. This region of strongest signal is vertically centered on the CCD. An average of 10 (5 after binning) vertical pixels, or 160 μm of the image, defines the temperature profiles presented here.

Performing accurate H_2 thermometry, especially at high temperatures, requires overcoming laser stability and signal-to-noise challenges associated with broadband pulses and spectra. For averaged results, each CARS spectrum is the average of 500 frames for the flame measurements and 200 frames for the heated flow measurements. This averaging provides an adequate CARS signal-to-noise ratio given the spectral and intensity instabilities in the broadband pump/Stokes pulses required to excite H_2 rotational Raman transitions from ~350 to ~2150 cm^{-1} simultaneously. Additionally, averaged results may be compared between the two thermometry methods (H_2 and N_2) for an assessment of accuracy, even though burner fluctuations have been observed and will reduce the single-shot precision. Shot-to-shot fluctuations in integrated intensity or energy at specific frequencies within the ultrabroadband pulse spectrum do not directly equate to precision errors in the CARS spectrum and temperature evaluation. Spectrally uniform intensity fluctuations should not affect the relative CARS peak areas or fitted temperatures. Also, the amplitude of each CARS signal peak depends on the pump/Stokes impulsive excitation, which includes contributions from all frequency pairs (likely with uncorrelated noise fluctuations) with differences equal to the S-branch transition. Therefore, precise relative peak amplitudes and evaluated temperatures may occur with spectral noise, and signals with large Raman shifts (fewer pump/Stokes combination frequencies) should be more sensitive to noise. Each data set includes two additional spectra, averaged over the corresponding number of frames as the CARS signal data: a background

spectrum recorded without pump/Stokes illumination, and a nonresonant spectrum generated in a flow of methane at τ = 0. Background-subtracted CARS spectra are divided by background-subtracted nonresonant spectra to account for the spectral sensitivity of the experiment (pulse bandwidth, phase-matching, optical coatings, and spectral responsivity of grating and detector) before fitting to model CARS spectra (Section II.C). The wide frequency spacing of H_2 rotational peaks can generate CARS spectra at low temperatures with very few populated transitions or at high temperatures with populated transitions at large Raman shifts where the pump/Stokes bandwidth limits the excitation profile. The nonresonant third-order susceptibility of methane is relatively high (more than 2.5 times that of Ar, N_2, or O_2),[29] which enables us to collect nonresonant spectra with the signal levels across the H_2 frequency window necessary for H_2 temperature measurements.

C. Rotational CARS modeling

The focus of this work is on H_2 RCARS, but we also present N_2 RCARS results to assess and validate H_2 thermometry. The bulk of this section outlines the modeling and fitting procedures for H_2 spectra, and differences in these procedures for CARS of N_2 or H_2/N_2 mixtures are addressed at the end of the section. The time-domain CARS signal calculations presented here are similar to previous methods.[18, 30] While the experimental probe pulse electric field is included explicitly in this model, the pump and Stokes interaction pulse is assumed to be transform limited and a delta function in time. Therefore, we divide the experimental CARS spectra by a nonresonant spectrum (Section II.B.), which serves as a spectral responsivity function, to account for the experimental deviation from infinite bandwidth of Raman state preparation in the model. In these experiments, the probe follows the pump/Stokes pulse at a delay, τ , that is large enough to assure no pulse

overlap or nonresonant signal contributions. The time-domain CARS signal simplifies to the time-dependent Raman-resonant signal with polarizability, calculated as

$$\chi(t) = \sum_{\Delta J=+2} W_{JJ'} \exp\left[\left(i\omega_{JJ'} - 2\Gamma_J\right)t\right]. \quad (1)$$

In Eq. (1), $\chi(t)$ is the sum of contributions from Stokes transitions from states J to $J' = J + 2$, where J is the angular-momentum quantum number. These transitions occur at positive $\omega_{JJ'}$ Raman frequencies, which are calculated from differences between rotational energies, $F(J+2) - F(J)$, where

$$F(J) = B_{v=0}J(J+1) - D_{v=0}J^2(J+1)^2 + H_{v=0}J^3(J+1)^3, \quad (2)$$

with ground vibrational state rotational constants from Ref. [31]. The J-dependent Raman linewidths, Γ_J, in Eq. (1) model the collisional dephasing and are given by the Lorentzian half-width at half maximum (HWHM) of the Raman transition. Following a treatment similar to those of Refs. 3-4, 7, we express the Raman linewidths as

$$\Gamma_J = 2\pi D_0(T)\nu_{JJ'}^2 / c\rho + \gamma_J(T)\rho, \quad (3)$$

where $D_0 = 0.01176T^{0.8314}$ cm^{2}amagat/s is the temperature-dependent optical diffusion coefficient,[3] $\nu_{JJ'}$ are the Raman transition frequencies in cm^{-1} ($\nu_{JJ'} = \omega_{JJ'} / 2\pi c$), c is the speed of light, ρ is the density, and $\gamma_J(T) = \tilde{\gamma}_J T + \gamma_0$ is the temperature-dependent collisional broadening coefficient in units of cm^{-1}amagat^{-1} with $\tilde{\gamma}_J$ and γ_0 values taken from Table 1 of Ref. 4. Removing the J-dependence of γ_J results in 1% lower evaluated temperatures, on average, over a 340–800 K range. Note that the wavenumber units of Γ_J from Eq. (3) must be converted to radial frequency units for Eq. (1). Finally, the $W_{JJ'}$ terms in Eq. (1) are weighting functions that, for treatment of an individual species, are simply

$$W_{JJ'} = (N_{J'} - N_J) b_{JJ'} F_J, \tag{4}$$

where N_J ($N_{J'}$) are the temperature-dependent rotational Boltzmann population distribution fractions for the J (J') state, $b_{JJ'}$ are the Placzek-Teller coefficients, and F_J are the Herman-Wallis factors. For the Stokes transitions ($J' = J + 2$) in the experiments presented here, the Placzek-Teller coefficients are given by

$$b_{J,J+2} = \frac{3(J+1)(J+2)}{2(2J+3)(2J+1)}. \tag{5}$$

The Herman-Wallis factors, which account for vibration-rotation interaction, are as follows:[32-34]

$$F_J = \left[1 + \frac{\eta^2}{\chi}(J^2 + 3J + 3)\right]^2, \tag{6}$$

where the variable χ is defined as the ratio of anisotropic polarizability expansion coefficients[32-33] and is distinct from $\chi(t)$ in Eq. (1). In Eq. (6), $\chi = 0.38$ for the H_2 S-branch,[33] and $\eta = 2B_e / \omega_e$ includes the rotational constant ($B_e = 60.8$ cm^{-1}) and vibrational frequency ($\omega_e = 4401$ cm^{-1}) of H_2.[35] For the H_2 S-branch transitions in this work, the F_J factors increase from 1.01 to 1.50 for transitions out of initial states $J = 0$ to $J = 9$, respectively. The rigid rotor approximation ($F_J = 1$ for all J transitions) results in falsely high evaluated temperatures; the error increases with temperature, e.g., 1% near room temperature to 4% near 800 K.

Using the calculated Raman-resonant polarizability, $\chi(t)$, and probe experimental pulse parameters, we model the experimental H_2 CARS spectrum at several temperatures from 200 K to >2000 K to include in a library for fitting. Boltzmann fractions (Eq. (4)) dominate the intrinsic temperature dependence of $\chi(t)$, but linewidths (Eq. (3)) also contribute. For example, fixing Γ_J (J) from Eq. (3) to constant values calculated at T=600 K, the actual dependence of Γ_J on T results

in evaluated temperature errors up to 5% for a set of 300–800 K spectra when the linewidths are not properly calculated. The set of Stokes transitions out of initial states $J=[0,9]$ is included in the Eq. (1) summation of $\chi(t)$ and is sufficient to describe the H_2 Raman spectrum for all temperatures measured in this work. The experimental probe pulse is assumed to be transform limited with electric field amplitude, $E_{pr}=\sqrt{I_{pr}}$, where the intensity cross-correlation of the femtosecond pump/Stokes and picosecond probe pulses is considered to be equal to I_{pr}. Given the carrier frequency, ω_0, and delay, τ, of the probe, we can express the CARS time-domain electric field as,[18]

$$E_{CARS}(t-\tau)=E_{pr}(t-\tau)\exp[i\omega_0(t-\tau)]\times\chi(t). \quad (7)$$

A Fourier transform with respect to *t* of Eq. (7) yields the complex-valued frequency-domain E_{CARS} field, and the square modulus of this field is the CARS spectrum, $I_{CARS}(\omega+\omega_0)$, which is shifted by ω_0 from $I_{CARS}(\omega)$. Modeled $I_{CARS}(\omega)$ spectra at 300 and 2000 K illustrate the large spectral bandwidth and strong temperature dependence of the $J=[0,9]$ H_2 transitions (Fig. 2). Additionally, the characteristic 9:1 intensity alternation exists between odd and even transitions, which is related to the nuclear spin statistics of H_2.

In this work, the fitting of an experimental CARS spectrum to the temperature library of model spectra involves the comparison of sets of *J*-indexed peak areas. In this context, an experimental CARS spectrum exists at each row of a CARS spectral image from the 2D array detector; each row spectrum can be fit to a model CARS spectrum (e.g., Fig. 2). Compared to alternate methods of fitting one complete spectrum with another,[18] the peak area fitting strategy has advantages of relaxing both the calibration requirement of the experimental detection axis and the consistent wavelength assignment of spectral peaks with asymmetric and varying pixel sensitivity functions

due to grating spectrometer coma and other aberrations.[36-38] A nonlinear least-squares algorithm is used to find the temperature library model spectrum that minimizes the residual between sets of experimental and model peak areas, which have been treated in the following manner: the set of experimental peak areas is normalized to its maximum; a set of model peak areas has the total area under peaks scaled to that under the set of normalized experimental peaks. Interpolation of the library temperatures yields a fit to the nearest 0.5 K.

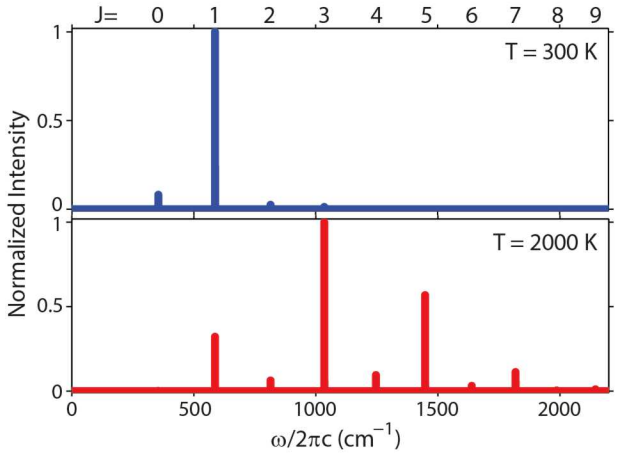

FIG. 2. The height-normalized set of pure-rotational H_2 CARS transitions out of initial states $J = [0, 9]$ are simulated for two temperatures: 300 K (top panel, blue) and 2000 K (bottom panel, red).

The N_2 RCARS model and experimental fitting differ from the H_2 methods in the following aspects. To fit the temperatures measured in this work, the N_2 model includes the set of Stokes transitions out of initial states $J = [0, 40]$ in Eq. (1). In our experiments, spectral filtering of the CARS signal from the probe limits fitting to detected lines $J = [4, 40]$; furthermore the use of a 600 grooves/mm grating for simultaneous N_2 and H_2 collection reduces the spectral resolution and restricts fitting to the higher nuclear spin-weighted transitions out of even-numbered initial J states. Instead of calculating the Γ_J using Eq. (3), we take the temperature-dependent linewidths from those previously obtained from time-domain coherence measurements[39] and then interpolate to the spectral library temperatures. Additionally, the N_2 model incorporates Herman-Wallis factors that

differ from those of H_2, and the specific coefficients and constants in the right-hand side of Eq. (6) are taken from Ref. [40] for N_2. Finally, collisions between H_2 and N_2 molecules in mixtures affect the linewidth of each molecule. We modify our H_2 and N_2 CARS spectral models by incorporating species-specific, concentration-weighted linewidth sums in a method that has been shown to result in more accurate evaluations of temperature.[4, 41] The N_2 thermometry model combines the N_2-N_2 linewidths[39] and experimental N_2-H_2 linewidths;[41] the H_2 model requires additional $\tilde{\gamma}_J$ and γ_0 values[4] to calculate $\gamma_J^{H_2\text{-}H_2}(T)$ and $\gamma_J^{H_2\text{-}N_2}(T)$, which are then combined to solve Eq. (3) for Γ_J.

III. RESULTS AND DISCUSSION

The temperature profiles presented below are for H_2 and N_2 CARS thermometry of a heated flow and diffusion flame. For these demonstration experiments with repetition rates defined in Section II.A, averaged results are presented along with the corresponding single-shot precisions that help determine the potential for H_2 CARS measurements in transient turbulent combustion processes. The temperature traces are obtained using the following procedure: the experimental spectrum from each CCD row is fit to the appropriate model (Section II.C.); the fitted temperatures are averaged over 5 (2x2 binned) vertical pixels (160 μm) in the peak signal region ~3.5 mm above the surface of the flow or burner. This procedure is repeated for each thermocouple-measured temperature (heated flow, Section III.A.) or lateral position (Wolfhard-Parker slot burner, Section III.B.) to create temperature profiles for thermometry comparison.

A. Heated flow CARS thermometry

For the heated-flow mixture of H_2 and N_2, RCARS spectra are collected with a 600 grooves/mm grating, which assures the detection of the complete set of H_2 S-branch transitions

while retaining the minimum resolution needed for N_2 S-branch temperature fitting. Extracted temperature profiles from fitting a single set of data are shown in Fig. 3(a) for H_2 (red trace) and N_2 (black dotted trace). The x-axes in Fig. 3(a,b) represent the set temperatures of the flow, as measured by a thermocouple (type K, 240 μm diameter) centered at the flow exit. Since the actual temperature at the center of the flow exit may differ from the set temperature, we first assess the H_2 RCARS thermometric accuracy by comparison with the simultaneously collected N_2 RCARS data. The fs/ps RCARS technique has been well benchmarked for accuracy previously with N_2.[30, 42-44] We calculate the magnitudes of H_2 and N_2 temperature differences (gray trace in Fig. 3(a), expressed as percentage of thermocouple-measured set temperature) and find that the H_2 and N_2 temperature profiles demonstrate good agreement. The average difference is 16.5 K (3.0%) over the full range (room temperature through ~800 K) with all differences <6.7% (Fig. 3(a)). While good agreement is thus demonstrated, there is still room for improvement. In repeated day-to-day measurements, the low-temperature region from 290-350 K proves to be the most difficult, and the evaluated H_2 temperature can differ from the fitted N_2 temperature by as much as 20% near 300 K in an otherwise accurate data set; at and above 350 K, temperature evaluations are far more robust. The evaluated H_2 temperatures are quite sensitive to the exact excitation profile and its recovery, which reduces the reproducibly of accurate low-temperature measurements. As mentioned previously, the more drastic change of the H_2 versus N_2 S-branch spectra with temperature might imply that H_2 is a more sensitive molecule for thermometry. However, this benefit is counterbalanced by the increased influence of shot noise errors on temperature fitting for H_2, which has only ~1/5 of the number of populated transitions as N_2 at a given temperature in these experiments.

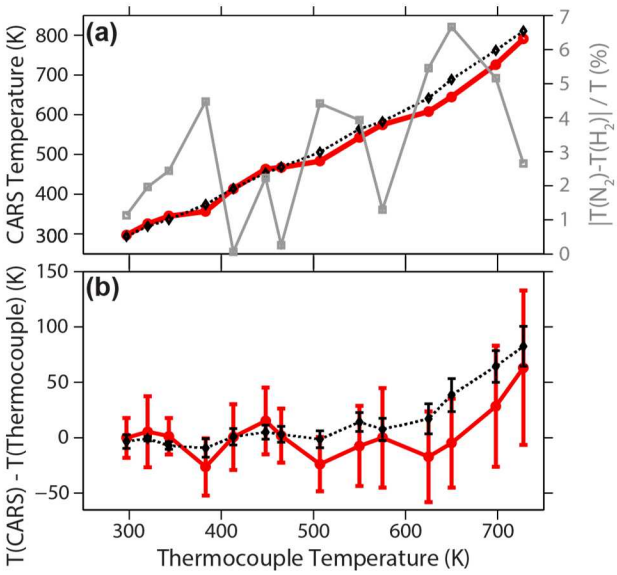

FIG. 3. Evaluated temperatures and statistics of heated flow CARS spectra taken at a series of thermocouple-measured set temperatures. (a) Temperatures extracted from pure-rotational CARS models are plotted for H_2 (red trace) and N_2 (dotted black trace) measured simultaneously (600 grooves/mm grating). Absolute values of the differences between H_2 and N_2 temperatures are plotted as percentages of thermocouple set temperatures (gray trace, right axis). (b) Differences between fitted temperatures and set temperatures are shown for H_2 (red trace) and N_2 (dotted black trace). The ±σ error bars give the single-shot precision of H_2 and N_2 RCARS thermometry measurements.

The H_2 and N_2 temperature profiles closely match the set temperature through ~650 K, which is evident in temperature differential plots for each molecule (Fig. 3(b)). At temperatures in excess of 650 K, the thermocouple readout was systematically lower than both the N_2 and H_2 evaluated temperatures, in which case the comparison between the benchmark N_2 data provides the best assessment of the accuracy of the H_2 thermometry data. The average deviations of the N_2 temperature from the thermocouple are 18.2 K (2.9%) over the full temperature range and 9.0 K (1.7%) for set temperatures ≤650 K. The residuals for H_2 for the corresponding temperature ranges are similar: 14.0 K (2.5%) and 8.7 K (1.9%). In repeated averaged-shot experiments and among individual laser shots, we find that the reproducibility of the H_2 thermometry near room temperature is difficult, because with only two intense rotational transitions (Fig. 2, top panel), even subtle fluctuations in excitation efficiency significantly affect the evaluated temperature. One possible solution would be to collect the experimental and nonresonant spectra simultaneously,

and this is currently under development in our laboratory. For single-laser-shot implementation of RCARS H_2 thermometry, such a referencing scheme could help improve the single-shot precision of evaluated temperatures to match that of RCARS N_2 thermometry. For our current experiment, the standard deviations of 200 single-shot spectral temperature fits are given as red (black) error bars for H_2 (N_2) in Fig. 3(b) for each set temperature. The N_2 thermometry yields smaller error bars on average (σ = 1.8% of the mean fitted temperature), but H_2 also provides fairly high precision with σ = 6.8% of the mean. The use of temperature fits to quantify indirectly the laser pulse fluctuations is motivated by the impulsive excitation (see Section II.B) and signal-probe frequency nondegeneracy of hybrid CARS. One other quantifier of relevant experimental noise is the ratio of two dominant peak amplitudes within the H_2 S-branch; this ratio has an average shot-to-shot standard deviation of 15%. Our aim in this work is to provide an assessment of the viability of H_2 wideband S-branch thermometry, and improvements in the overall precision of single-shot measurements are planned by incorporating single-shot corrections for the excitation profile.

B. Diffusion flame CARS thermometry

For the Wolfhard-Parker burner measurements, two sets of CARS spectra are collected from the N_2-seeded H_2 diffusion flame that is translated laterally across the fixed probe volume. Like in the heated flow case, a dataset detected with the 600 grooves/mm grating can be used for simultaneous thermometry of the two species. Figure 4(a) is a spectrum from a ~1200 K point in the flame that has been fitted for temperature using $J = [0, 7]$ H_2 and $J = [4, 40]$ N_2 transitions; magnification levels emphasize the disparity of signal intensity between N_2 and H_2 and across the H_2 series due to a combination of transition strength, excitation efficiency (dashed trace, Fig. 4(a)), and density of molecules. Resulting temperature profiles discussed later in this section are truncated in flame regions where low signal-to-noise levels prevent temperature fitting of one

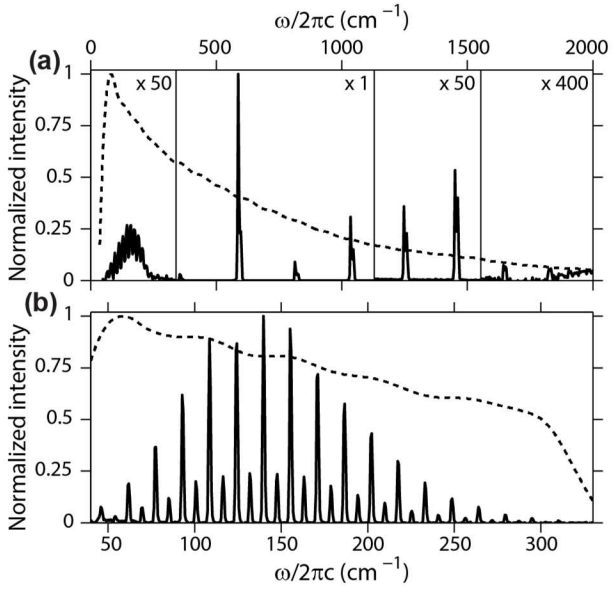

FIG. 4. Experimental RCARS spectra in diffusion flame (~1200 K), probed at y = 3.5 mm above burner surface and x = 3.15 mm from fuel slot center. (a) Lower resolution RCARS spectrum (solid lines) contains N_2 rotational transitions below 350 cm^{-1} and H_2 transitions out of $J = 0$ (~354 cm^{-1}) through $J = 7$ (1818 cm^{-1}) states. After overall height normalization, the labeled magnification is applied to each spectral region. (b) Higher resolution, height-normalized RCARS spectrum (solid lines) of N_2 rotational transitions out of $J = 4$ (~44 cm^{-1}) through $J = 40$ (327 cm^{-1}) states. (a,b) Height-normalized nonresonant methane spectra (dashed lines) are overlaid.

molecule. In this experiment, the detected H_2 signal disappears at peak flame temperatures and also outside of the fuel slot where no H_2 is present. Above the fuel slot and away from the air slot, N_2-seeding of the H_2 fuel is necessary to detect the N_2 S-branch spectrum. Even with seeding, the N_2 signal is low on the fuel side of the flame (Fig. 4(a)). The region between flame walls produces CARS spectra with much stronger H_2 than N_2 transitions, because of the 21:4 H_2:N_2 flow rate ratio, probe delay (160 ps), and broad pump/Stokes spectrum. The attenuation via neutral density filters necessary to avoid CCD saturation of H_2 lines results in N_2 lines that are too weak for temperature fitting. Sacrificing simultaneous species thermometry between flame walls and focusing only on the unattenuated N_2 spectrum still poses the challenge of scattering within the spectrometer of the extremely strong, low-temperature, low-frequency H_2 transitions into the CCD image of the N_2 S-branch. High-resolution N_2 spectra characterizing the complete burner surface are detected after a 2400 grooves/mm spectrometer grating and a spectral filter to eliminate H_2 transitions. Resulting

spectrally filtered N_2 RCARS and nonresonant spectra from this configuration are shown in Fig. 4(b), where the N_2 spectrum of $J=[4,40]$ Raman transitions is taken at an identical point in the flame as in Fig. 4(a). Thus, this high resolution dataset provides both a check for flame and laser pulse stability over the ~1 hour of data collection and validation of the reduced peak fitting procedure described in Section II.C. for N_2 RCARS thermometry using the lower resolution N_2 spectra.

In the absence of known temperatures at each flame position, we assess the performance of H_2 RCARS thermometry in a flame by comparison of H_2 and N_2 temperature profiles (Fig. 5). At each burner position, we calculate the residual temperature and percent error of the extracted H_2 or N_2 temperature (simultaneously collected spectra) with respect to the temperature extracted from the higher resolution N_2 spectra, which serves as the common reference. First, we determine the self-consistency of the N_2 temperature measurements between different datasets with the low and high resolution detection. Over the flame positions where the N_2 temperature profiles collected from low and high resolution gratings overlap, the average residual of N_2 temperatures (dotted black trace – blue trace, Fig. 5) is 34.7 K (4.0%), which reduces to 18.1 K (2.6%) with the removal of points at ~3.2 and ~6.3 mm locations within the steepest portions of the temperature profile. Possible explanations for the larger residuals at these locations include laser shot noise or positional reproducibility errors due to flame instability or translation stage motion. The overall agreement between these two N_2 data sets confirms the thermometry results from lower resolution N_2 spectra here and in the heated flow (Section III.A.) and justifies the comparison of H_2 and N_2 extracted temperatures from asynchronously collected spectra.

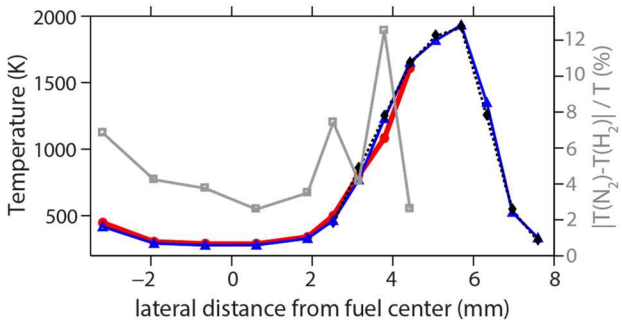

FIG. 5. Diffusion flame temperature profile spanning the burner fuel slot and one flame wall. CARS spectra are collected ~3.5 mm above the burner surface at a series of lateral burner positions. Temperatures extracted from models are plotted for H_2 (red trace) and N_2 (dotted black trace) measured simultaneously (600 grooves/mm grating) and for N_2 (blue trace) collected in higher resolution spectra (2400 grooves/mm grating). Differences between H_2 and N_2 temperatures are plotted as absolute value percentages of reference temperatures (gray trace, right axis).

The error of averaged H_2 temperatures by comparison to the averaged N_2 reference temperatures (red trace – blue trace, Fig. 5) serves to quantify the accuracy of our H_2 S-branch thermometry approach, and is plotted in gray in Fig. 5 as an absolute value percentage of the reference N_2 temperatures. Over the range of temperature profile overlap, the average H_2 residual is 36.3 K (5.3%). Despite the similarity to the average N_2 residual, the H_2 and N_2 residuals differ in magnitude and sign at common points, so the temperature profiles of simultaneously collected H_2 and N_2 spectra are not better matched. The standard deviation of extracted temperatures from a series of multiple-shot spectra is largest at the flame front positions, e.g., 3–4 mm from fuel center (Fig. 5). We can see from single-laser-shot assessments that the precision of the RCARS thermometry measurements is worse for the flame than for the previous heated flow both for N_2 and H_2 for all conditions. In the flame front, the precisions of H_2 and N_2 measurements are σ = 17% and σ = 14%, respectively. Therefore, the flame is operating with real fluctuations, and single-laser-shot statistical fluctuations are not a good representation of the precision of the technique itself.

V. CONCLUSION

We have demonstrated the feasibility and accuracy of H_2 RCARS thermometry by using it to measure temperatures in a heated flow and a diffusion flame. For each system, we compare temperatures extracted from the collected broadband H_2 S-branch CARS spectra to those extracted with well-established methods from N_2 S-branch CARS spectra. The recovered H_2 and N_2 temperatures are, on average, within 3.0% of each other over a temperature range of 290–800 K in a heated flow and within 5.3% over 290–1610 K in a diffusion flame. Additionally, our assessment of H_2 and N_2 thermometry accuracy requires the comparison of measured temperatures to set temperatures of the heated flow. For thermocouple readings ≤650 K, the measured temperatures are, on average, within 2% of the set temperature for N_2 and H_2. Finally, the H_2 temperature precisions over multiple averaged-shot spectra and for single-shot measurements are 3% and 6.8%, respectively. These results compare favorably with previous H_2 VCARS flame thermometry results of 4% repeated measurement precision, and 3% or even 5-10% error from N_2, thermocouple, or calculated temperatures.[16-17] In our work, differences in H_2 and N_2 results at low temperatures can arise from limited H_2 transitions for fitting, while a significant improvement in reproducibility is obtained at temperatures over approximately 350 K. Further, the chaotic nature of the supercontinuum generation scheme yields pulse-to-pulse spectral fluctuations that degrade the single-shot precision, and current work in our lab is targeted at developing a shot-to-shot correction for the varying excitation profile. The ability to measure the complete H_2 rotational distribution will be important to studies of non-equilibrium molecular energy transfer, where it has been shown that small molecules, such as H_2, may have persistent modal temperature differences during rapid energy release or relaxation of a gas ensemble including a larger collision partner, which is generally the case for H_2.[45]

In summary, we have performed H_2 RCARS thermometry across a wide temperature range at atmospheric pressure. Our experimental results and spectral model indicate the viability of using S-branch H_2 CARS spectra to directly probe temperatures in combustion reactions that occur under rich conditions. The accuracy and versatility of H_2 RCARS thermometry motivate the continued development of this laser diagnostics tool to characterize high-temperature chemical processes.

ACKNOWLEDGMENTS

This work was supported by the Division of Chemical Sciences, Geosciences, and Biosciences, the Office of Basic Energy Sciences (BES), the U.S. Department of Energy (DOE). Sandia National Laboratories is a multi-mission laboratory managed and operated by Sandia Corporation, a wholly owned subsidiary of Lockheed Martin Corporation, for the DOE's National Nuclear Security Administration under contract DE-AC04-94AL85000.

REFERENCES

1. A. C. Eckbreth, *Laser Diagnostics for Combustion Temperature and Species, Second Edition* (Taylor & Francis, New York, 1996).
2. C. J. Kliewer, Y. Gao, T. Seeger, J. Kiefer, B. D. Patterson, and T. B. Settersten, Proc. Combust. Inst. **33**, 831 (2011).
3. L. A. Rahn, R. L. Farrow, and G. J. Rosasco, Phys. Rev. A **43**, 6075 (1991).
4. H. Tran, P. Joubert, L. Bonamy, B. Lavorel, V. Renard, F. Chaussard, O. Faucher, and B. Sinardet, J. Chem. Phys. **122**, 194317 (2005).
5. W. D. Kulatilaka, P. S. Hsu, H. U. Stauffer, J. R. Gord, and S. Roy, Appl. Phys. Lett. **97**, 081112 (2010).
6. H. U. Stauffer, W. D. Kulatilaka, P. S. Hsu, J. R. Gord, and S. Roy, Appl. Optics **50**, A38 (2011).
7. T. Lang, K. L. Kompa, and M. Motzkus, Chem. Phys. Lett. **310**, 65 (1999).
8. H. Skenderović, T. Buckup, W. Wohlleben, and M. Motzkus, J. Raman Spectrosc. **33**, 866 (2002).
9. H. Tran, F. Chaussard, N. Le Cong, B. Lavorel, O. Faucher, and P. Joubert, J. Chem. Phys. **131**, 174310 (2009).
10. C. F. Kaminski and P. Ewart, Appl. Optics **36**, 731 (1997).
11. V. A. Shakhatov, O. De Pascale, M. Capitelli, K. Hassouni, G. Lombardi, and A. Gicquel, Phys. Plasmas **12**, 023504 (2005).

12. F. Grisch, P. Bouchardy, and W. Clauss, Aerosp. Sci. Technol. **7**, 317 (2003).
13. K. Muller-Dethlefs, M. Pealat, and J.-P. E. Taran, Ber. Bunsenges. Phys. Chem. **85**, 803 (1981).
14. V. Bergmann and W. Stricker, Appl. Phys. B **61**, 49 (1995).
15. R. Bombach, T. Gerber, B. Hemmerling, and W. Hubschmid, Appl. Phys. B **51**, 59 (1990).
16. J. A. Shirley, R. J. Hall, and A. C. Eckbreth, Investigation of the Feasibility of CARS Measurements in Scramjet Combustion. In *Proc. 16th JANNAF Combustion Mtg.*, CPIA Publication No. 308: Laurel, MD, 1979; Vol. II, pp 487.
17. R. D. Hancock, K. E. Bertagnolli, and R. P. Lucht, Combust. Flame **109**, 323 (1997).
18. S. P. Kearney, D. J. Scoglietti, and C. J. Kliewer, Opt. Express **21**, 12327 (2013).
19. F. Vestin and P. E. Bengtsson, Proc. Combust. Inst. **32**, 847 (2009).
20. C. E. Dedic, J. D. Miller, and T. R. Meyer, Opt. Lett. **39**, 6608 (2014).
21. W. Clauss, A. A. Ilyukhin, D. N. Kozlov, V. V. Smirnov, O. M. Stelmakh, and K. A. Vereschagin, Appl. Phys. B **62**, 279 (1996).
22. W. Clauss, D. N. Kozlov, R. L. Pykhov, V. V. Smirnov, O. M. Stelmakh, and K. A. Vereschagin, Appl. Phys. B **65**, 619 (1997).
23. A. Bohlin, B. D. Patterson, and C. J. Kliewer, J. Chem. Phys. **138**, 081102 (2013).
24. A. Bohlin and C. J. Kliewer, Appl. Phys. Lett. **105**, 161111 (2014).
25. A. Bohlin and C. J. Kliewer, J. Phys. Chem. Lett. **6**, 643 (2015).
26. H. G. Wolfhard and W. G. Parker, Proc. Phys. Soc. A **62**, 722 (1949).
27. Y. Gao, T. Seeger, and A. Leipertz, P. Combust. Inst. **35**, 3715 (2015).
28. J. D. Garman and D. Dunn-Rankin, Combust. Flame **115**, 481 (1998).
29. J. W. Hahn and E. S. Lee, J. Opt. Soc. Am. B **12**, 1021 (1995).
30. J. D. Miller, S. Roy, M. N. Slipchenko, J. R. Gord, and T. R. Meyer, Opt Express **19**, 15627 (2011).
31. I. F. Silvera, Rev. Mod. Phys. **52**, 393 (1980).
32. T. C. James and W. Klemperer, J. Chem. Phys. **31**, 130 (1959).
33. C. Asawaroengchai and G. M. Rosenblatt, J. Chem. Phys. **72**, 2664 (1980).
34. R. H. Tipping and J. F. Ogilvie, J. Raman Spectrosc. **15**, 38 (1984).
35. M. Marrocco, J. Raman Spectrosc. **40**, 741 (2009).
36. J. Reader, J. Opt. Soc. Am. **59**, 1189 (1969).
37. E. Hecht, *Optics* 2nd ed.; (Addison -Wesley, Reading, MA, 1990).
38. M. K. Yetzbacher, T. L. Courtney, W. K. Peters, K. A. Kitney, E. R. Smith, and D. M. Jonas, J. Opt. Soc. Am. B **27**, 1104 (2010).
39. C. J. Kliewer, A. Bohlin, E. Nordstrom, B. D. Patterson, P. E. Bengtsson, and T. B. Settersten, Appl. Phys. B **108**, 419 (2012).
40. A. Bohlin, P. E. Bengtsson, and M. Marrocco, J. Raman Spectrosc. **42**, 1843 (2011).
41. A. Bohlin, E. Nordstrom, B. D. Patterson, P. E. Bengtsson, and C. J. Kliewer, J. Chem. Phys. **137**, 074302 (2012).
42. J. D. Miller, C. E. Dedic, S. Roy, J. R. Gord, and T. R. Meyer, Opt. Express **20**, 5003 (2012).
43. A. Bohlin and C. J. Kliewer, J. Phys. Chem. Lett. **5**, 1243 (2014).
44. S. P. Kearney, Combust. Flame **162**, 1748 (2015).
45. A. J. McCaffery and R. J. Marsh, J. Chem. Phys. **136**, 024307 (2012).